Available online at www.sciencedirect.com
ScienceDirect
Cement and Concrete Research 37 (2007) 369–377
Cement and Concrete Research

MRI: A complementary tool for imaging cement pastes

S.J. Jaffer [a], C. Lemaire [b], C.M. Hansson [a,*], H. Peemoeller [b]

[a] Department of Mechanical Engineering, University of Waterloo, 200 University Avenue West, Waterloo, ON, Canada N2L 3G1
[b] Department of Physics, University of Waterloo, 200 University Avenue West, Waterloo, ON, Canada N2L 3G1

Received 3 October 2005; accepted 17 July 2006

Abstract

This study examined the advantages and limitations of imaging cement paste with magnetic resonance imaging (MRI) using the single point imaging (SPI) sequence. Cement paste samples made with low water to cement (w/c) ratios were examined. The resolutions that could be attained in the images depended on the sizes of the samples. This technique, however, proved to be sensitive to water concentration gradients and allowed monitoring of water diffusion into the paste samples. In order to calibrate the features of the MR image, a comparison was made between electron micrographs and MR images of the same specimens. This revealed that the former could produce higher resolution images, however, considerable time was needed for sample preparation, the sample integrity was not guaranteed and only a small area of the sample could be viewed. In contrast, MRI offered in situ images which were three-dimensional and took less time to obtain than the electron micrographs but were of lower resolution. It is concluded that MRI could be a valuable tool for imaging cement pastes provided the features of the images have been "calibrated" by comparison with other, better known, techniques.

Keywords: MRI single point imaging; SEM; Crack detection; Diffusion; Cement paste

1. Introduction

Unlike conventional microscopy techniques that enable two-dimensional (2-D) imaging of the solid phases, magnetic resonance imaging (MRI) offers a different perspective on the study of cement pastes. Important advantages of this technique are that it permits three-dimensional (3-D) imaging with minimal sample preparation and provides information on the liquid phases. Also, depending on the capability of the MRI spectrometer, paste samples can be examined in situ.

Publications that have documented imaging of cement pastes with MRI include those by Beyea et al. [1], Bogdan et al. [2] and Tritt-Goc et al. [3]. These studies have used one- and two-dimensional imaging over a given experiment time, which achieves significantly improved signal to noise (S/N) ratio compared to that in 3-D imaging because the former involves the projection of the whole sample information onto a line or a plane. A recent study by Young et al. [4] has involved 3-D imaging of cement paste which is also the focus of the present work.

An important aspect of MRI is that a paste sample can be imaged with different pulse sequences, each of which uses the relaxation time characteristics of a specific structure and phase present in the paste to enhance the contrast and/or the geometrical resolution in the image. Young et al. [4], for example, have combined the inversion recovery and the spin-echo sequence to suppress the signal from the solid components of the paste in order to improve the signal to noise (S/N) ratio of a water-filled synthetic crack in their sample compared to that using the spin echo sequence alone.

In the present study, the basic single point imaging (SPI) sequence [5] has been applied to 3-D imaging of cement pastes. The purpose of this paper is to discuss the advantages and limitations of imaging cement pastes using SPI, and to show how other imaging techniques could be used to "calibrate" features observed in the MR images.

2. Background

In SPI, initially proposed by Emid and Creyghton [5], the gradients along the x-, y- and z-axes (G_x, G_y and G_z) are activated before a short broadband radio frequency (rf) pulse is

* Corresponding author. Tel.: +1 519 888 4538.
E-mail address: chansson@uwaterloo.ca (C.M. Hansson).

0008-8846/$ - see front matter © 2006 Elsevier Ltd. All rights reserved.
doi:10.1016/j.cemconres.2006.07.003

applied which rotates the net magnetization that is originally in the direction of the magnetic field by 90°. The gradient along one of the axes, say G_x along the x-axis, is then changed in steps while the other gradients are kept constant. In this way, the density of spins, as a function of x, is phase encoded along the gradient direction of G_x, so that a particular phase in the NMR signal corresponds to a particular position on the x-axis. This process is then repeated consecutively for the other two axes ensuring all three dimensions are encoded. It should be noted that spins start dephasing after the application of the 90° pulse and the detection of signals takes place at a time, t_c, thereafter. The signals are then Fourier transformed to form the final spatial image. The signal obtained in an MR image is proportional to the density of the spins and is modulated by effective spin-spin relaxation time, T_2*. The asterisk signifies that the observed, or effective, T_2 is involved and may be different from the characteristic sample T_2 due to inhomogeneities in the main magnetic field. This signal is also affected by the spin-lattice relaxation time, T_1. The magnetization T_1 saturation level is a function of the time, TR, between two consecutive applications of the pulse sequence (also know as repetition time), and the effective rotation angle, α, of the net magnetization by the rf pulse, which is not always exactly 90° (this pulse is nominally 90°; in practice it is a smaller α pulse determined by the frequency bandwidth requirement of the selected resolution, and the broad line characteristics of the free induction decay). Using TR, α and t_c, optimum resolution can be achieved for the various structures found in the cement samples, each with its own characteristic relaxation times T_1 and T_2. More details about SPI contrast can be found in [6,7].

In porous materials, a commonly used connection between pore sizes and relaxation times is given by Eqs. (1) and (2) for T_1 and T_2, respectively [8,9];

$$\frac{1}{T_1} = \rho_1 \frac{S}{V} + \frac{1}{T_{1b}} \quad (1)$$

$$\frac{1}{T_2} = \rho_2 \frac{S}{V} + \frac{1}{T_{2b}} \quad (2)$$

where S/V is the surface to volume ratios of the pores and ρ_1 and ρ_2 are the spin–lattice and spin–spin surface relaxivity constants, respectively. T_{1b} and T_{2b} are the bulk water spin relaxation times. For pure water protons, T_{1b} and T_{2b} values are approximately equal to 3 s. In cement, these equations may be further complicated by the fact that the pore solution contains a high concentration of paramagnetic ions. The magnetic interaction between the water molecule spins and the ion spins has the effect of reducing the bulk spin relaxation times and increasing surface relaxivities. Water molecules of solvation undergo rotational motion with correlation times comparable to that of pure water, of the order of ps, but usually their residence times in the coordination shell of the ions are longer then their residence times anywhere else in the bulk water, also of the order of ps. Effectively the residence times express a slowdown of the translational motion of water molecules around the ions, exposing them to longer proton–ion interaction. Values for both rotational and residence correlation times have been measured or simulated for many ions species, including Mg^{2+} and Ca^{2+} [10]. The concentration of ions in the pore solution of white cement pastes, as determined by Mammoliti [11], is given in Table 1. Also, nuclear magnetic resonance (NMR) measurements conducted by Greener et al. [12] on paste samples made with white cement revealed a magnetization component with $T_2 \approx 40$ ms at about 12 min after mixing. According to Greener et al. [12], this component represents the proportion of the mixing water that has not yet formed a part of the hydration products. This T_2 is very short compared to that of free water (3 s) and its value is attributed to the influence of water proton–ion interactions.

Table 1
Concentration of elements in pore solution [11]

Element/Compound	Concentration (mg/L)
SiO_2	*<D.L.*
Al	*<D.L.*
Fe	*<D.L.*
Ca	490
Mg	0.6
Na	3760
K	1770
S	43.6
Cl	26.9

For species indicated in italics concentrations were below detection limit of the technique.

Table 2
Composition of Aalborg white cement used (courtesy of LCM, EPFL, Switzerland)

Compound	% in Aalborg
Alite (C_3S)	68.5
Belite (C_2S)	17.1
C_3A	7.6
C_4AF	0.0
CaO	0.6
MgO	0.7
Gypsum ($C\bar{S}H_2$)	2.7
Semihydrate ($C\bar{S}H_{1/2}$)	0.6
Anhydrite ($C\bar{S}$)	0.4
$CaCO_3$	0.9
CH	0.5
SiO_2	0.6

3. Experimental procedures

3.1. Instrumentation and methods

3.1.1. Magnetic Resonance Imaging (MRI)

The MRI system used for this study was a DMX 500 MHz, 11.74 Tesla, Bruker microimaging spectrometer. The SPI sequence implemented for imaging was provided with the spectrometer. The SPI phase encoding technique was employed to avoid susceptibility artefact from the strong magnetic field. Two imaging probes, Micro 2.5 and Micro 5, containing the rf and gradient coils were used and each was singly tuned to hydrogen (proton resonance). The Micro 2.5 probe had a 30 mm diameter (ϕ) rf coil and the Micro 5 could be adjusted to hold a

2, 5 or 10 mm ϕ rf coil. The images were displayed on a computer using Paravision software Version 2.11.

For most 3-D scans, the imaging matrix was 64 × 64 × 32 data points in size and each scan was obtained from 32 averages for a total scan time of 11 h; it must be noted here that since the S/N is significantly reduced for the high resolution images, we have chosen to consider the time as an expendable variable to get the observed resolution. However, the highest resolution images were obtained in a 2 mm ϕ coil, and were achieved with a 64 × 64 × 64 imaging matrix, 32 accumulations and a total scan time of about 40 h. In addition, some low-resolution 32 × 32 × 32 scans with 8 accumulations were acquired in about 45 min. 2-D images were obtained using a 64 × 64 window and 16 accumulations in about 5 min. SPI, being a 3-D phase encoding technique, is inherently slow compared to other MRI sequences but has the important advantage of being free of susceptibility artefacts. This is an essential feature for accurate high resolution imaging of short T_2* mineral material. Increasing scan times improve the signal to noise, as well as T_1 and T_2 contrast. For all but the highest resolution imaging sessions, t_c and TR were 150 μs and 10 ms, respectively; for the highest resolution scans, they were 237 μs and 18 ms. The longer t_c used in the latter case was chosen in accordance with the maximum gradient available. TR was kept at 10 ms in most cases to reduce T_1 saturation effects caused by shorter repetition times. Also the angle α of the RF pulse was set at 6°.

The value of t_c = 150 μs was shorter than the T_2 of gel water in fully hardened white cement (200 μs) observed by Holly et al. [13] implying that both gel and capillary water (H_2O) could be readily detected in well hydrated pastes. The protons (hydrogen ions) found in solid calcium aluminate phases and in hydroxyl (OH) groups of calcium hydroxide (CH) and calcium silicate hydrates (C–S–H) could not be identified because their T_2 of 20 μs was shorter than the detection limit. Similarly, water in the interlayers of C–S–H with a T_2 of 100 μs could not be detected.

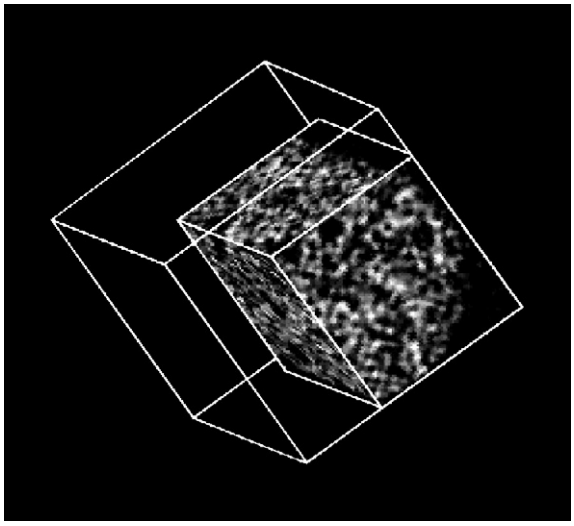

Fig. 1. A 3-D MR image of cement paste with a resolution of 10 μm along each of the three orthogonal axes. The large box on the outside (640 μm × 640 μm × 640 μm) shows the actual scan boundary. The scanned image occupied this box. The sides of the smaller inner box were adjusted to show this particular view inside the sample.

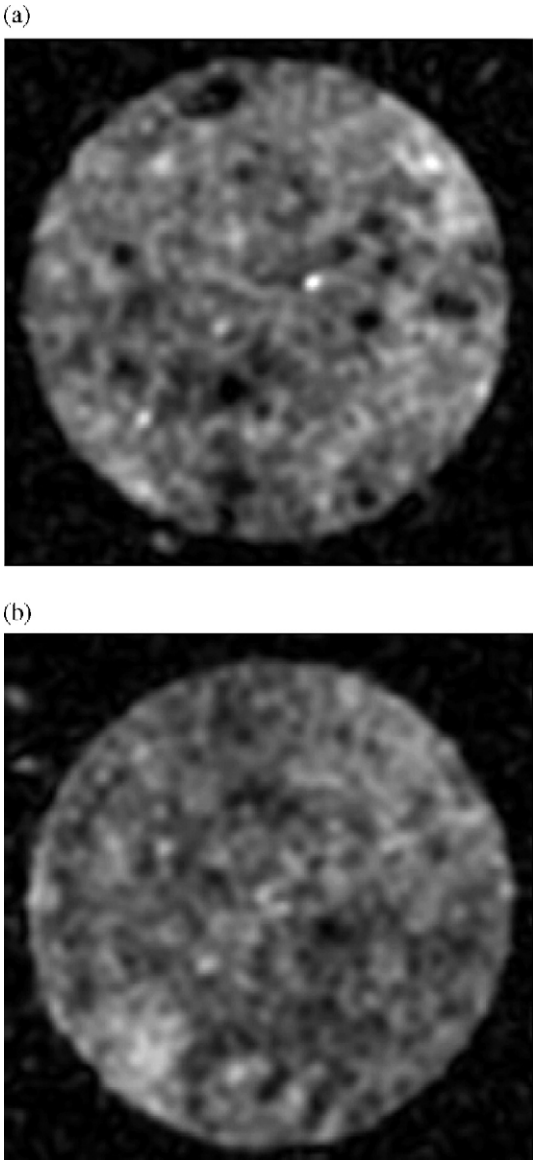

Fig. 2. Axial slices taken at 10 mm from the top surface from a 3-D MR image of a mechanically cracked 20 mm ϕ paste sample made with D_2O (w/c) after exposure to H_2O for (a) 1 h and (b) 3 h.

3.1.2. Environmental scanning electron microscopy (ESEM)

The ESEM used was Electroscan E-3, which was connected to the computer containing Link ISIS Rev 1.04a software from Oxford Instruments. The electron beam power was maintained at 20 keV. The secondary electron (SE) and backscattered electron (BSE) modes were used for imaging. For backscattered electron (BSE) imaging sample surfaces were ground and polished before they were inserted in the electron microscope. Water pressure maintained in the specimen chamber was 3.5 and 0.7 Torr for SE and BSE modes, respectively.

3.2. Sample preparation

All cement paste samples were made with Aalborg white cement with the composition given in Table 2. Some of the samples were mixed with distilled water (H_2O) while others

were made with deuterium oxide (D_2O or "heavy water"). The latter was used because a deuterium nucleus is not detected when the MRI system is set for proton resonance. The idea behind this was that, if H_2O were allowed to penetrate into the cracks and defects in hardened sample made with D_2O, they would be clearly detectable and distinguishable from the deuterated products of hydration [14]. All but two samples were made with a water (H_2O or D_2O) to cement (w/c) ratio of 0.35: the two exceptions were made with a w/c ratio of 0.25. The purpose of making samples with such low w/c ratios was to encourage self-desiccation of the hydrating paste and study the effects of post-hardening absorption of water. Immediately after mixing, the pastes were placed in 20 mm, 10 mm and 5 mm ϕ glass MRI sample tubes which were sealed to prevent loss or absorption of moisture from the atmosphere and where the paste was allowed to set and harden.

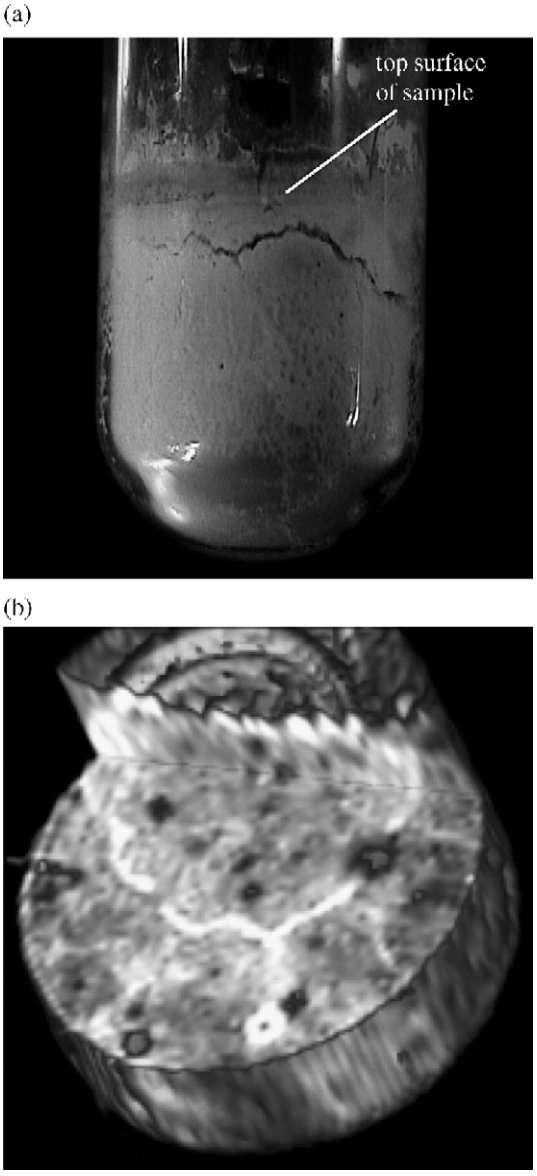

Fig. 3. (a) A photograph of a 20 mm ϕ mechanically cracked paste sample inside the test tube it was cast in and (b) a 3-D MR image of the sample displaying its inside. The bright rings on the top surface of the MR image are from a test tube filled with H_2O which was left on top of the sample to prevent it from drying out while it was being scanned.

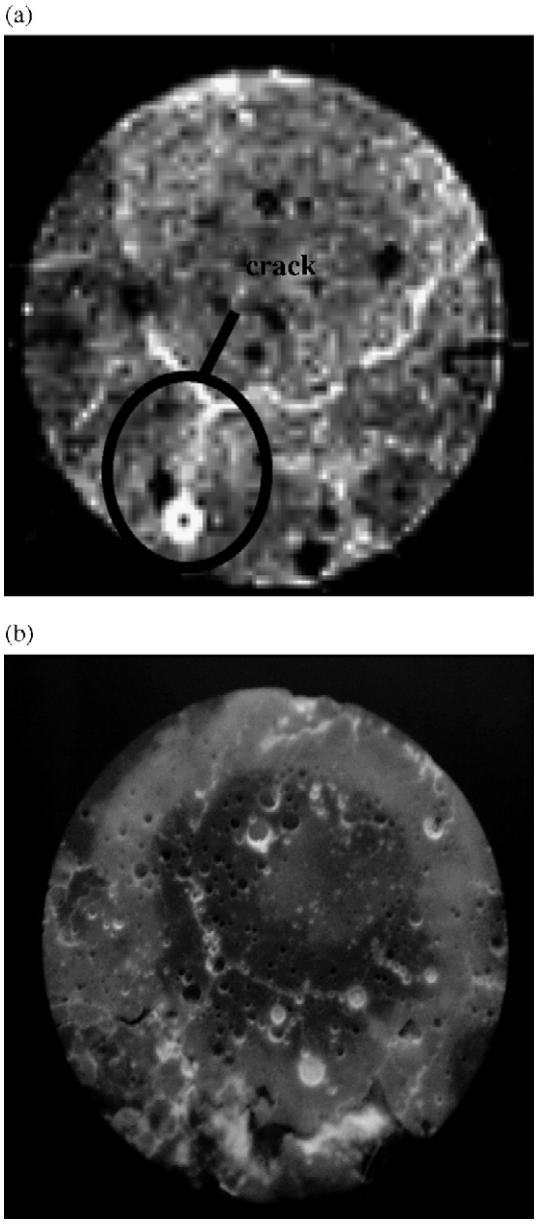

Fig. 4. (a) An axial slice obtained from the 3-D MR image in Fig. 3 of the 20 mm ϕ specimen and (b) a macrograph taken using a camera. These images were obtained at 2 mm from the top surface of the sample.

Most samples were imaged using the MRI spectrometer while still in the sample tubes at 8 days after mixing. One exception was an H_2O-paste 5 mm ϕ samples (w/c 0.35), which was demoulded one day after it was prepared and was placed in H_2O for 28 days to examine the effect of the long immersion period on its microstructure. The other exception was one of the deuterated samples that was removed from its broken sample tube and placed in a specially made Teflon holder. Preliminary tests indicated that, if the specimens were not saturated with H_2O before they were imaged, it was difficult to obtain a good S/N ratio in the image, irrespective of whether they were made with H_2O or D_2O. Therefore, H_2O was poured on the top

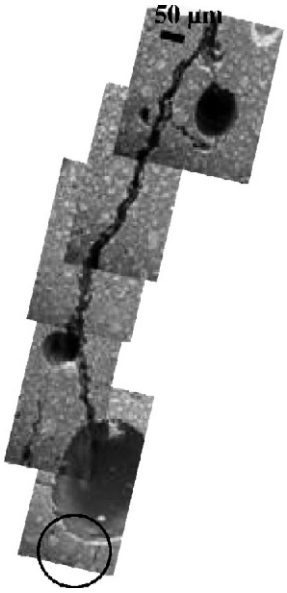

Fig. 5. A mosaic of BSE ESEM images to show part of the crack marked in Fig. 4(a). Circled area contains a 10 μm width crack.

surface of all the latter samples for about 6 h before they were placed in the spectrometer except for the D_2O-paste sample (w/c 0.25) in the Teflon sample holder for which the water was poured on the sample surface in intervals and the sample was scanned after each interval.

For electron microscopy, a mechanically cracked H_2O-paste sample (w/c = 0.25) was dried under atmospheric conditions for approximately 11 months to remove excess water introduced during MRI experiments and was impregnated with Spurr epoxy [15], a low viscosity epoxy that penetrated deeper into the sample than other epoxies. Fluorescent dye was added to the Spurr epoxy in order to allow the defects in the sample to be observed under UV light.

4. Results and discussion

To obtain higher resolution images using MRI, the sample size had to be significantly reduced. The highest resolution obtained was 10 μm × 10 μm × 10 μm/voxel for a paste sample of about 0.3 mm^3 that had been cut out of the 5 mm ϕ sample immersed in water for 28 days. Fig. 1 shows a 3-D image of this sample. The light areas in this image and all other MR images in this section indicate H_2O filled spaces (e.g. capillary pores, gel pores).

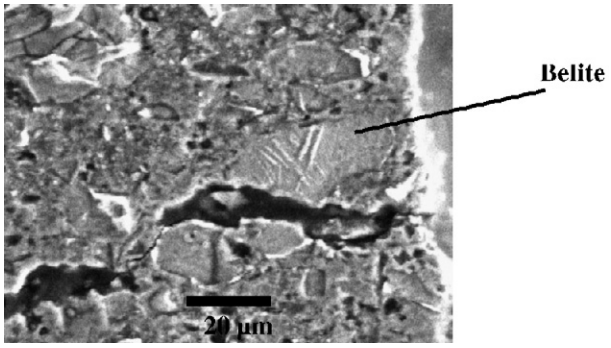

Fig. 6. A higher resolution image of the 10 μm cracks shown in Fig. 5 showing a disintegrated belite phase.

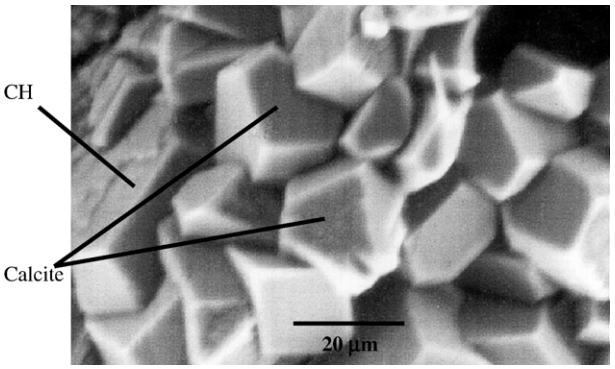

Fig. 7. An SE ESEM image showing CH and calcite crystals in a sample similar to the one imaged in Fig. 1.

When larger samples were imaged, the resolution that could be attained in the images was reduced accordingly. The best practical resolution that could be attained for 20 mm, 10 mm and 5 mm ϕ samples was 312 μm × 312 μm × 624 μm/voxel, 148 μm × 148 μm × 296 μm/voxel and 86 μm × 86 μm × 172 μm/voxel, respectively. No self-desiccation cracks were observed in these samples at these resolutions, regardless of the w/c ratio used. The possible reasons for this are (i) the crack widths could have been below the resolution limit of the MRI experiment, (ii) the small sample size could have prevented self-desiccation cracks from forming or (iii) if cracks did exist and were filled with water, the exchange with the surrounding paste during the long scan times could have caused the cracks to lose their contrast with respect to the surrounding cement matrix, making them undetectable. The size resolution problem is also encountered in another 3-D imaging technique, namely X-ray computed tomography (CT) [16]. However, with CT, the variations in a sample's structure can be identified based only on the material density distribution in the sample, while with MRI the samples are examined using measures of density and

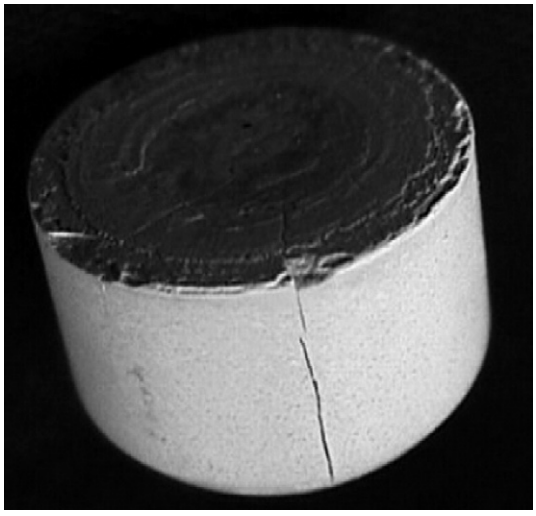

Fig. 8. Photograph of a cracked 20 mm ϕ paste sample made with D_2O (w/c = 0.25).

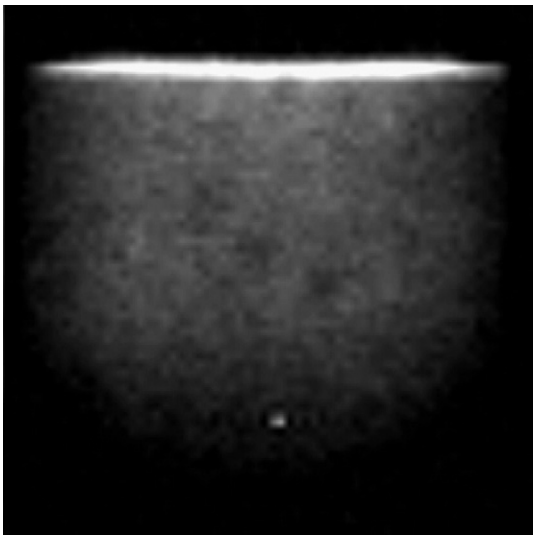

Fig. 9. A 2-D MRI projection of the sample in Fig. 8 after it was exposed to water for 1 h on its top surface.

dynamics. In addition, nuclei other than hydrogen (e.g. ^{2}H, ^{17}O, ^{35}Cl, ^{129}Xe) can be used as probes but consideration of S/N (such as abundance of isotope relative to hydrogen and the concentration of the species) may limit image resolution for nuclei other than hydrogen. Cano et al. [17], for instance, have used the single point 1-D SPRITE imaging technique to study the penetration of ^{23}Na and ^{35}Cl in Portland cement mortar.

If the chosen fluid containing the probe nuclei reacts with the solid component of cement, this process could also be monitored with MRI as is the case for water. To understand this concept, Fig. 2 (a) and (b) shows axial (cross-section) slices taken from 3-D images of a 20 mm ϕ mechanically cracked sample made with D_2O (w/c 0.25). These slices were taken at 10 mm from the top surface of the sample and were obtained after exposing the top surface to water for a total of 1 and 3 h, respectively. The image in Fig. 2(a) has a slightly higher overall brightness than that in Fig. 2 (b) which can be attributed to the fact that more of the water in the former has not formed a part of the hydration products. Moreover, it has a different distribution of water with a larger amount of black areas corresponding to unhydrated cement.

The aspect of MRI that is particularly valuable is the 3-D in situ imaging. This requires minimal sample preparation and minimizes damage to the sample. Fig. 3(a) shows a photograph of a mechanically cracked cement sample made with a w/c (H_2O) ratio of 0.25 inside the sample tube in which it was cast. Fig. 3(b) illustrates the 3-D image of this sample while still in the sample tube. An axial slice taken from this image at 2 mm from the top surface using MRI is shown in Fig. 4(a). The specimen was then impregnated with epoxy containing a fluorescent dye, removed from the sample tube, and ground and polished to approximately the same depth as that of the MR image in Fig. 4(a). A macrograph of this plane taken under fluorescent light is shown in Fig. 4(b). Features seen in the macrograph are clearly resolvable in the MR image. In fact, porous areas are better identified in the MR image than in the macrograph because closed pores were not impregnated by epoxy. Moreover, the preparation steps required for the epoxy-impregnated sample have led to some disintegration along its edges even though considerable care was taken to minimize damage.

Fig. 5 shows a mosaic of various ESEM images of the crack encircled in Fig. 4(a). ESEM images give very detailed information about the microstructure in the paste. In this particular image, cracks with a width of about 10 μm can easily be identified but are not distinguishable in the MRI slice. Higher resolution images from the ESEM, such as that in Fig. 6, also enable the identification of the different phases in cement paste, for example the belite particle labelled in the micrograph.

A major disadvantage of the ESEM evaluation is that it is very time consuming: (i) up to 6 days of sample preparation to allow the epoxy to penetrate the specimen (ii) many hours of imaging time when identifying the location and interconnectivity of the crack network on one plane in the sample, imaging it piece by piece and integrating the images. To obtain a 3-D image, this latter process must be repeated by grinding off layers,

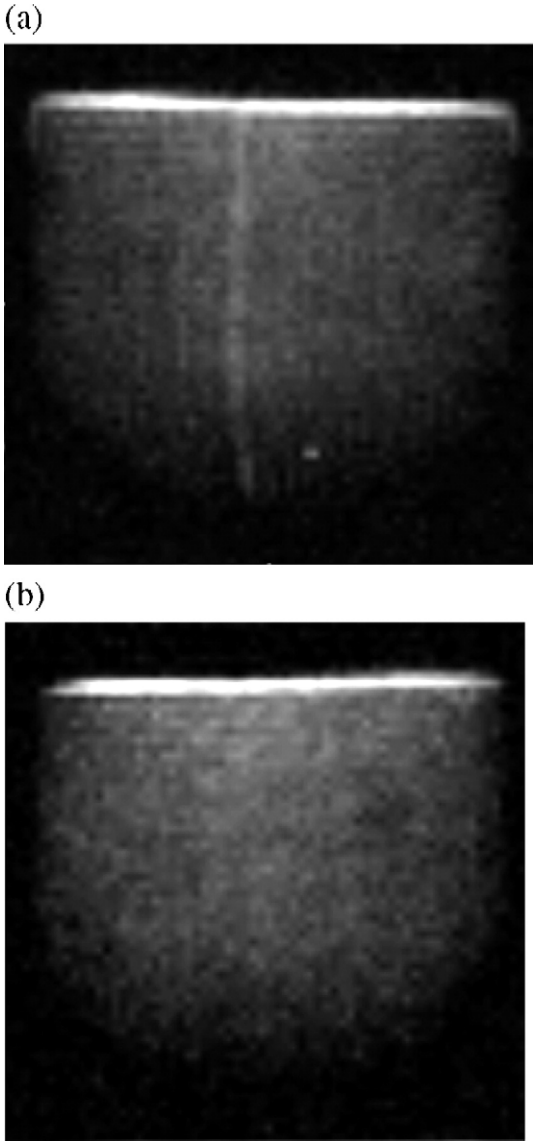

Fig. 10. 2D MRI projections of the sample in Fig. 8 after an additional 2 h of exposure of top surface to water. (a) and (b) show the sample in the same orientation and were taken about 11 h apart.

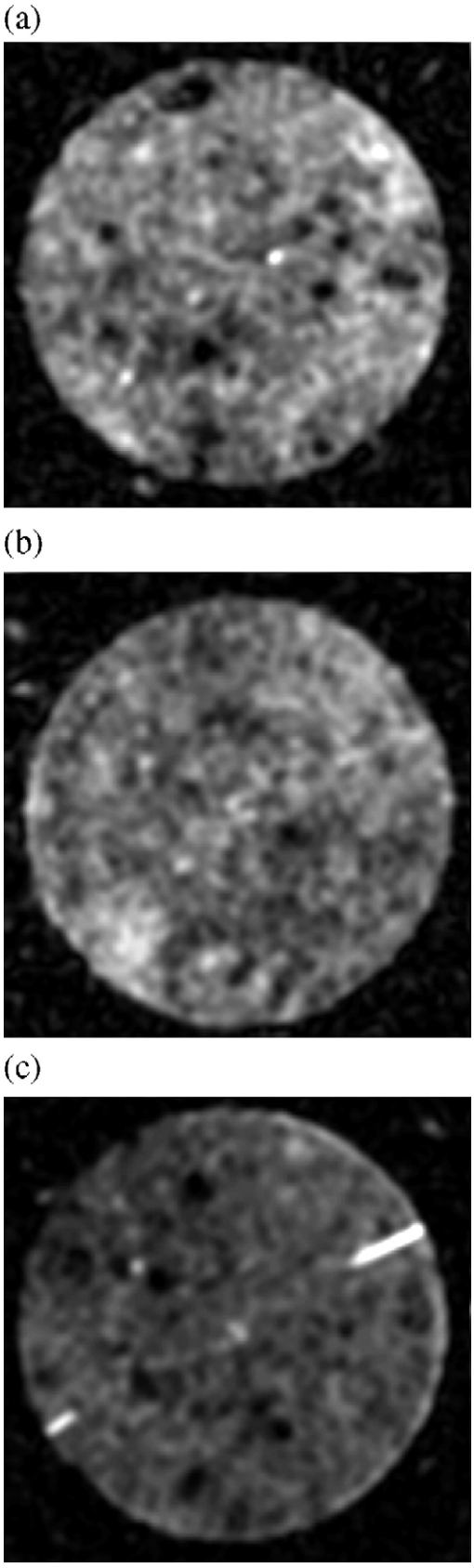

Fig. 11. Axial MRI slices taken at 10 mm from the top surface of the sample at (a) 1 h, (b) an additional 2 h and (c) an additional 3 h of exposure of the top surface to water. The contrast values were kept constant for all three images.

imaging each layer and then reconstructing a 3-D image. Using this process, ESEM analysis is destructive and prevents longitudinal studies of the samples. By comparison MRI is non-destructive. MRI, which is less time consuming, can be used as a complementary technique in this case. For example, 2 h of MRI setup time and the scan time of 11 h in the case of the 3-D MR image shown in Fig. 3 gives a reasonable image in which the major cracks and their interconnectivity in the sample can be identified. However, a calibration of MR images by information obtained from ESEM images is required in this case to be able to interpret the former. For instance, the dark regions on the front surface of the MR image shown in Fig. 1 were identified as CH and calcite crystals using ESEM and shown in Fig. 7. The calcite would have been formed by the carbonation of the sample while it was being imaged.

In this project, H_2O was added to the surface of the sample and allowed to penetrate into the defects in the cement paste. For a 20 mm ϕ D_2O-paste sample that was mechanically cracked as shown in Fig. 8, H_2O was left on the surface of the sample in

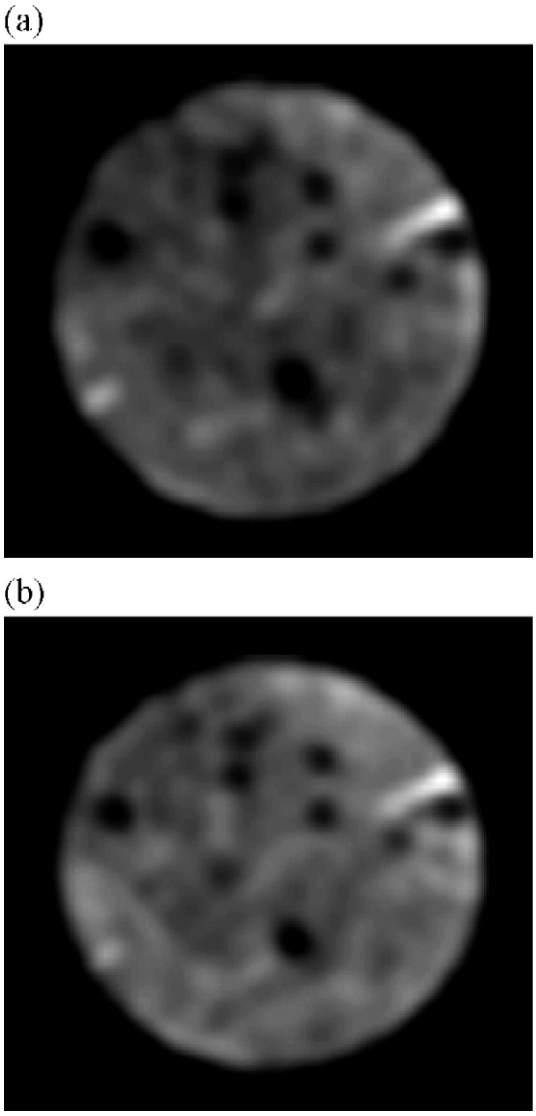

Fig. 12. Axial slices from 3-D low resolution MRI scans of the D_2O sample in Fig. 8 taken 13 h apart. (a) was obtained before (b).

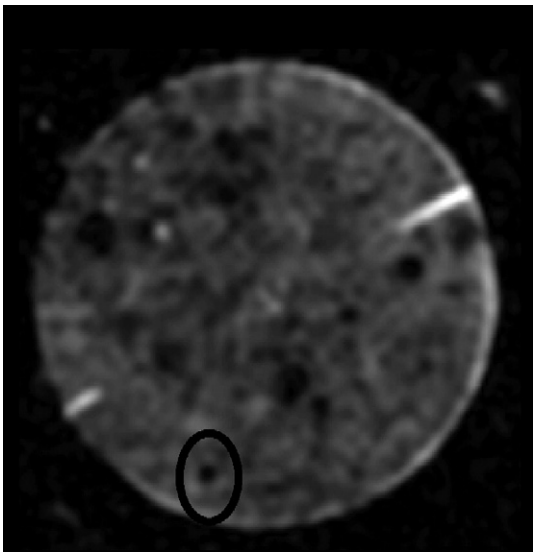

Fig. 13. An axial slice from a 3-D high resolution MRI scan of the D_2O sample in Fig. 8. Encircled black spot cannot be found in the images presented in Fig. 12.

intervals and then excess H_2O was removed from the top surface and the sample was scanned after each interval. After H_2O had been left on the surface of the sample for 1 h, the 2-D projection of the sample, presented in Fig. 9 showed no visible cracks in the sample. After water had been left for an additional 2 h on the surface of the sample, however, the 2-D projection in Fig. 10(a) clearly showed a crack through the sample. In a similar projection taken 11 h later and shown in Fig. 10(b), the crack was no longer visible. A comparison of Fig. 10(a) and (b) shows that there was a larger amount of water in most of the paste after 11 h which was likely due to absorption from the crack. The amount of time water is left on the surface of the sample prior to the MRI measurements and the duration of the scan are, thus, very important as cement paste has the tendency to absorb water and, if not fully hydrated, to further react. This is particularly true of young pastes, or specimens made with low w/c ratios. On the other hand, if water is not left on the sample for a sufficient period of time, especially in the case of specimens mixed with D_2O, the S/N ratio becomes a problem [14]. Fig. 11 shows axial slices at 10 mm from the top surface obtained from 3-D images of the same sample exposed to water for different intervals. The slices are shown at the same contrast (grey) level. The image in Fig. 11(a) taken after 1 h surface exposure to H_2O has comparable S/N ratio to that of the image in Fig. 11 (b) taken after an additional 2 h of surface exposure to water, as indicated by the similarity in background noise in both the images. Compared to these two images, the image in Fig. 11(c), taken after an additional 3 h of exposure to water, gives the higher S/N ratio. Hence, a balance between S/N ratio and the hydration of cement paste must be attained and may vary from sample to sample.

Lower resolution images that take a short time to achieve can be very valuable when it comes to determining the diffusion into, and distribution of, water in the sample. This is especially applicable to cases in which the sample is scanned for higher resolution images that take a long time during which the sample evolves. Fig. 12 shows axial slices from 3-D low resolutions scans of the cracked D_2O sample shown in Fig. 8 after it was exposed to water for 6 h. The two scans, each of which was 45 min long, were taken about 13 h apart. Between these two scans, a long duration (about 11 h), higher-resolution 3-D scan was taken. The two short duration scans show the evolution of the sample while it was undergoing high resolution scanning. Water has diffused more into this slice even though excess water on the top surface of the sample was removed. Moreover, the reduction in sizes of the unhydrated cement particles (the black areas in the figures) by further hydration is clearly discernable. Long duration, high-resolution scans can be useful for identifying features that are not clear from the low resolution scans such as the unhydrated particle shown by the encircled black area in Fig. 13, which is not detectable in Fig. 12(a) and (b).

5. Conclusions

It can be concluded from the above that MR imaging has far more advantages than limitations. Its major limitation is that, to obtain high resolution images, the sample size must be very small and the scan time fairly long. However, this limitation is overshadowed by its ability to obtain 3-D in-situ images with minimum sample preparation, and without sample destruction, which allows for longitudinal studies. It is very sensitive to water concentration gradients and allows monitoring of diffusion of water into the paste sample. Nuclei other than protons can be used as probes in the sample. With more detailed "calibration" of the MRI images by information from other techniques, it is predicted that MRI will prove to be a valuable tool for studies of hydration, diffusion, permeation and structural defects in cements pastes.

Acknowledgements

The authors would like express their gratitude to the Natural Sciences and Engineering Research Council (NSERC) of Canada for funding this project. Technical assistance extended by Dr. M. Ioannidis and Dr. R. Holly is greatly appreciated.

References

[1] S.D. Beyea, B.J. Balcom, T.W. Bremner, P.J. Prado, A.R. Cross, R.L Armstrong, P.E. Grattan-Bellew, The influence of shrinkage-cracking on the drying behaviour of white Portland cement using single-point imaging (SPI), Solid State Nuclear Magnetic Resonance 13 (1-2) (1998) 93–100.

[2] M. Bogdan, B.J. Balcom, T.W. Bremner, R.L. Armstrong, Single-point imaging of partially dried, hydrated white Portland cement, Journal of Magnetic Resonance 116 (2) (1995) 266–269.

[3] J. Tritt-Goc, J. Pislewski, S. Koscielski, F. Milia, The Influence of the superplasticiser on the hydration and freezing processes in white cement Studied by ^1H spin-lattice relaxation time and single point imaging, Cement and Concrete Research 30 (6) (2000) 931–936.

[4] J.J. Young, P. Szomolanyi, T.W. Bremner, B.J. Balcom, Magnetic resonance imaging of crack formation in hydrated cement paste materials, Cement and Concrete Research 34 (8) (2004) 1459–1466.

[5] S. Emid, J.N.H. Creyghton, High resolution NMR imaging in solids, Physica. B, Condensed Matter 128 (1) (1985) 81–83.

[6] P. Jezzard, J.J. Attard, T.A. Carpenter, L.D. Hall, Nuclear magnetic resonance imaging in solid state, Progress in NMR Spectroscopy 23 (1) (1991) 1–41.

[7] S.D. Beyea, B.J. Balcom, P.J. Prado, A.R. Cross, C.B. Kennedy, Relaxation time mapping of short T_2* nuclei with single-point imaging (SPI) method, Journal of Magnetic Resonance 135 (1) (1998) 156–164.
[8] J. Korringa, D.O. Seevers, C.H. Torrey, Theory of spin pumping and relaxation in systems with a low concentration of electron spin resonance centers, Physical Review 127 (4) (1962) 1143–1150.
[9] R.L. Kleinberg, W.E. Kenyon, P.P. Mitra, Mechanism of NMR relaxation of fluids in rock, Journal of Magnetic Resonance. Series A 108 (2) (1994) 206–214.
[10] H. Ohtaki, T. Radnai, Structure and dynamics of hydrated ions, Chemical Reviews 93 (3) (1993) 1157–1204.
[11] L. Mammoliti, Examination of the mechanism of corrosion inhibition by $Ca(NO_2)_2$-and $Ca(NO_3)_2$-based admixtures in concrete, Ph.D. Thesis, 2001, University of Waterloo: Waterloo, Ontario, Canada.
[12] J. Greener, H. Peemoeller, C. Choi, R. Holly, E.J. Reardon, C.M. Hansson, M.M. Pintar, Monitoring of hydration of white cement paste with proton NMR spin–spin relaxation, Journal of the American Ceramic Society 83 (3) (2000) 623–627.
[13] R. Holly, Characterization of white cement paste: effect of temperature and chemical corrosion inhibitor, Ph.D. Thesis, 2000, University of Waterloo: Waterloo, Ontario, Canada.
[14] C. Choi, J. Peternelj, M.M. Pintar, A method for measuring the diffusivity of a liquid into a porous matrix, Journal of Chemical Physics 109 (5) (1998) 1860–1862.
[15] A.R. Spurr, A low-viscosity epoxy resin embedding medium for electron microscopy, Journal of Ultrastructure Research 26 (1969) 31–43.
[16] M.C. Garci Juenger, "X-ray vision" for cement-based materials, Concrete International 26 (12) (2004) 38–41.
[17] F.J. Cano, T.W. Bremmer, R.P. McGregor, B.J. Balcom, Magnetic resonance ^{1}H, ^{23}Na, and ^{35}Cl penetration in Portland cement mortar, Cement and Concrete Research 32 (2002) 1067–1070.